Electronic Supplementary Material (ESI) for New Journal of Chemistry.

Supporting Information

Ascorbic acid modified dual-metal-organic-framework derived C-Fe/Fe_3O_4 loaded on N-doped graphene framework for enhanced electrocatalytic oxygen reduction

Yating Zhang*[a,b], Nana Zhang[a], Lei Shen[a], Gang Lin[a], Pei He[a], Ke Suo[a], Ting Zhang[a], Xiaobo Wang[a], Keke Li[a]

[a]College of Chemistry and Chemical Engineering, Xi'an University of Science and Technology, Xi'an 710054, China;

[b]Key Laboratory of Coal Resources Exploration and Comprehensive Utilization, Ministry of Land and Resources, Xi'an 710021, China

* Corresponding author: zhangyt@xust.edu.cn (Y.T. Zhang)

1. Characterization of material

The morphologies of the catalysts were tested using a scanning electron microscope (SEM, Sirion 200). The particle size and internal structure of products were researched via transmission electron microscopy (TEM, FEI, Tecnai-F20). X-ray diffraction (XRD) patterns were measured via X-ray diffractometer (Bruker D8 Advance) with Cu-Kα radiation. Raman spectra were implemented on an invia Reflex spectrometer with an excitation wavelength of 532 nm. The surface area of products was computed by the Brunauer-Emmett-Teller (BET) method in the adsorption data. The X-ray photoelectron spectroscopy was implemented by virtue of the ThermoFisher K-Alpha instrument.

2. Electrochemical performance evaluation

The electrochemical properties of the ORR were performed on the 760D electrochemical workstation. The three electrode system is made up of an Ag/AgCl (reference electrode), a Pt wire (counter electrode), a glass carbon electrode (GCE, working electrode). The preparation process of working electrode is as follows: 5.0 mg catalyst tested was mixed in 1 mL of 5% Nafion (100 μL), ethanol (450 μL) and water (450 μL) followed by ultrasonication for 30 min. Afterward, 10 μL of the above ink was dripped into the well-polished glassy carbon electrode using a microliter syringe, and then let it dry naturally. The loading capacity of all catalysts and the benchmark Pt/C catalyst is calculated as follows: The diameter of the glass carbon electrode is 5 mm, and its area is about 0.196 cm^2. The concentration of catalyst ink is 5 mg/mL. For CVs and LSV test, drop 0.01 mL catalyst ink, and the catalyst load is: 5*0.01/0.196≈0.25 mg/cm^2. All electrochemical measurements were performed in O_2- or N_2-saturated 0.1 M KOH. Then, cyclic voltammograms (CVs) were measured between -0.8 and 0.2 V to activate the catalysts. The linear sweep voltammograms (LSV) were conducted at different electrode speeds from 400 to 2500 rpm.

The ORR dynamics can be analyzed using the Koutecky-Levich (K-L) equations:

$$\frac{1}{j} = \frac{1}{j_k} + \frac{1}{B\omega^{\frac{1}{2}}} \quad (1)$$

$$B = 0.2nFC_0D_0^{\frac{2}{3}}v^{\frac{-1}{6}} \quad (2)$$

In which, j_k and ω are kinetic current density on RDE and the rotating speed of the RDE, respectively. F is the Faraday constant (96485 C·mol^{-1}), D_0 is the diffusion coefficient of O_2 in

0.1 M KOH (1.9×10^{-5} cm^2 s^{-1}), v is the kinetic viscosity of the electrolyte (1.2×10^{-6}mol cm^{-3}), and C_0 is the concentration of O_2.

The RRDE test was implemented via LSV from 0.2 to -1 V versus Ag/AgCl with a scanning speed of 10 mV s^{-1} at 1600 rpm. Meanwhile the ring electrode was maintained at 1.3 V versus RHE. The number of transferred electrons (n) and the percentage of hydrogen peroxide (H_2O_2) were counted by using the following formula:

$$H_2O_2\% = 200\frac{I_r/N}{I_d+I_r/N} \quad (3)$$

$$n = 4\frac{I_d}{I_d+I_r/N} \quad (4)$$

Here, I_d refers to the disk current, I_r refers to the ring current, and N symbolizes the collection coefficient of the platinum wire (N = 0.37).

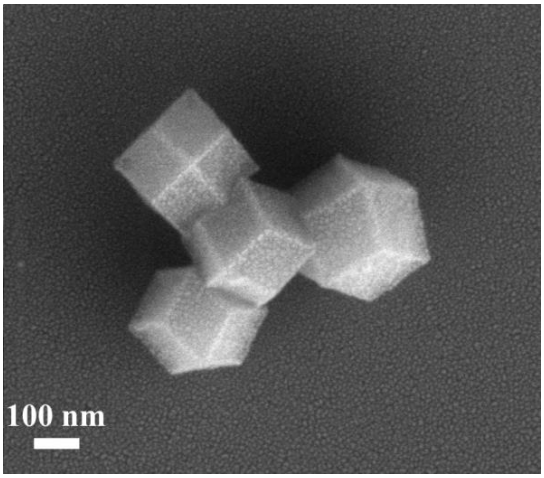

Fig. S1. The SEM images of Fe/Zn-MOFs.

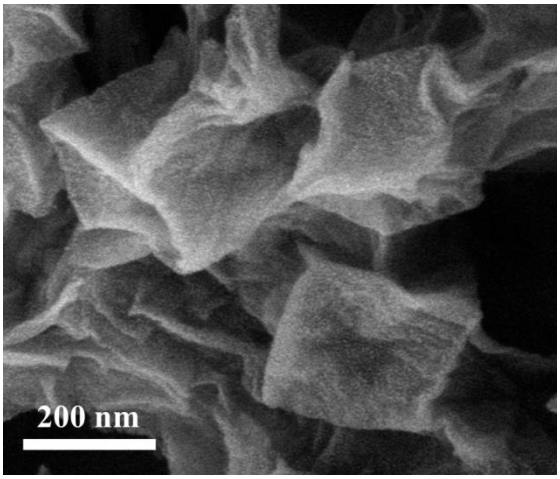

Fig. S2. The SEM images of C-Fe/Zn-MOFs@GO.

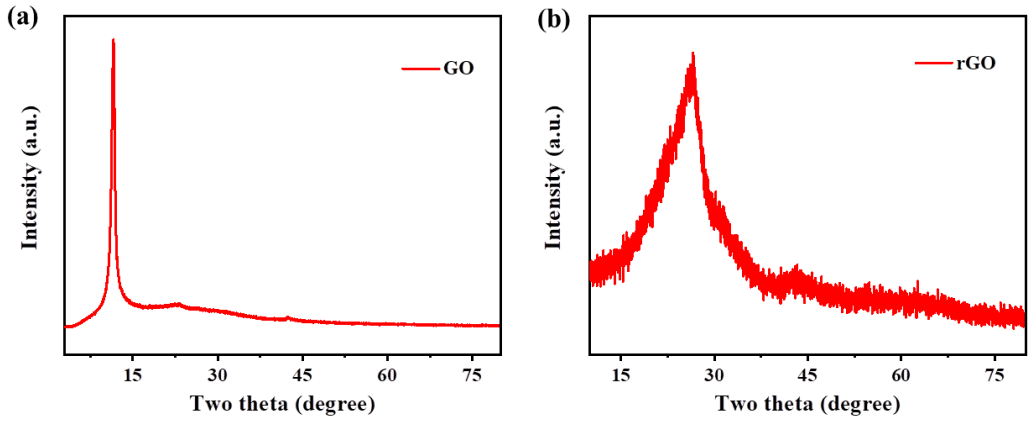

Fig. S3. XRD patterns of (a) GO and (b) rGO.

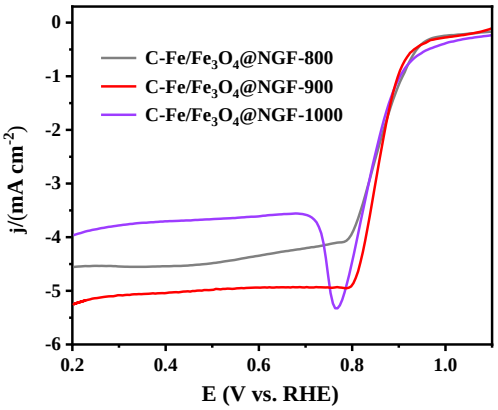

Fig. S4. LSV curves of C-Fe/Fe_3O_4@NGF at different temperatures.

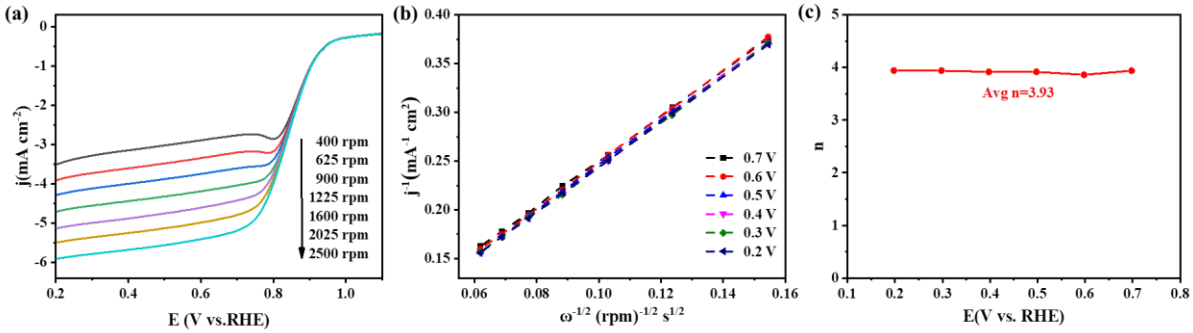

Fig. S5. (a) LSV curves of C-Fe/Fe_3O_4 catalyst recorded at different rotation rates. (b) Corresponding Kouteck-Levich plots derived from the RDE data. (c) The calculated electron transfer number derived from Kouteck-Levich plots.

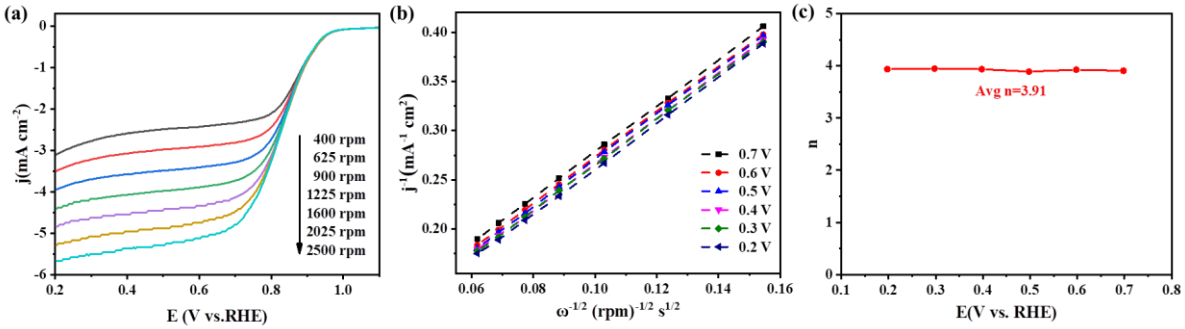

Fig. S6. (a) LSV curves of Fe/Fe_3O_4@NGF catalyst recorded at different rotation rates. (b) Corresponding Kouteck-Levich plots derived from the RDE data. (c) The calculated electron transfer number derived from Kouteck-Levich plots.

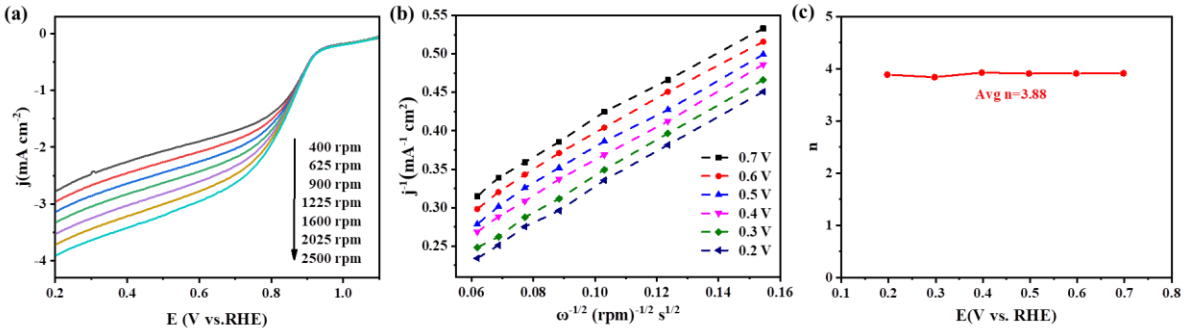

Fig. S7. (a) LSV curves of Fe/Fe_3O_4 catalyst recorded at different rotation rates. (b) Corresponding Kouteck-Levich plots derived from the RDE data. (c) The calculated electron transfer number derived from Kouteck-Levich plots.

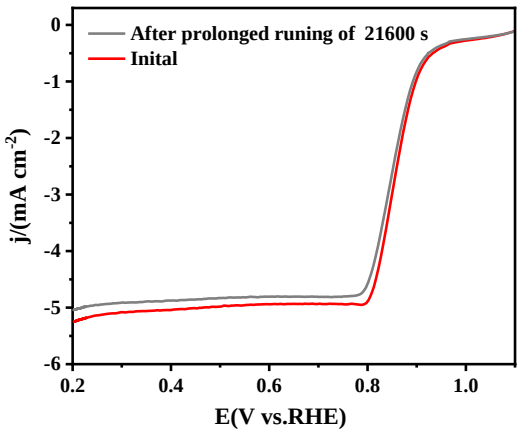

Fig. S8. LSV curves of C-Fe/Fe_3O_4@NGF before and after stability tests.

Table. S1 Comparison of ORR performance under alkaline conditions for our synthesized sample with other reported benchmark catalysts.

catalyst	ORR activity (0.1 M KOH solution)			Ref
	CV *vs.* RHE / V	E_{onset} *vs.* RHE / V	$E_{1/2}$ *vs.* RHE / V	
Co_3Fe_7-PCNF-850	0.83 V		0.85 V	[1]
H-Fe-N_x-C		1.05 V	0.92 V	[2]
Co/N CCPC-3	0.752 V	0.921 V	0.827 V	[3]
Fe@N-CNTs@rGO	0.769 V		0.83 V	[4]
a-Fe_2O_3/Fe_3O_4/hNCNC	0.82 V	1.030 V	0.838 V	[5]
N-Co_3O_4@NC-2		0.89 V	0.77 V	[6]
Co-N/CNFs		0.92 V	0.82 V	[7]
Ni-NC700	0.73 V	0.86 V	0.75 V	[8]
Fe_{20}@N/HCSs		-	0.86 V	[9]
Co,N-C900	0.88 V	0.97 V	0.85 V	[10]
Fe_3O_4@NHCSs		0.952 V	0.822 V	[11]
L-CCNTs-Co-800	0.79 V	0.90 V	0.84 V	[12]
Co@BNCNTs-900	0.83 V	0.93 V	0.82 V	[13]
Fe_3C-Co/NC	0.82 V	0.94 V	0.885 V	[14]
Co/N-CNTs@$Ti_3C_2T_x$	0.80 V	0.936 V	0.815 V	[15]
NG800		0.88 V	0.76 V	[16]
N-hG	0.77 V	0.91 V	0.833 V	[17]
COP@K10-Fe-900	0.816 V	0.97 V	0.85 V	[18]
N-Co_3O_4@NC-2		0.89 V	0.77 V	[19]
Co@N-CNTF-2	0.81 V	0.91 V	0.81 V	[20]
Co/N-BCNTs	0.80 V		0.83 V	[21]
CoZn-N-C-6	0.80 V	0.971 V	0.834 V	[22]
C-Fe/Fe_3O_4@NGF	**0.84 V**	**0.96 V**	**0.86 V**	**This Work**

References

[1] Liu M, He Y, Zhang J. Co_3Fe_7 nanoparticles encapsulated in porous nitrogen-doped carbon nanofibers as bifunctional electrocatalysts for rechargeable zinc–air batteries[J]. Materials Chemistry Frontiers, 2021, 5(17): 6559-6567.

[2] Yang H, Liu Y, Liu X, et al. Large-scale synthesis of N-doped carbon capsules supporting atomically dispersed iron for efficient oxygen reduction reaction electrocatalysis[J]. eScience, 2022.

[3] Wang T, He Y, Liu Y, et al. A ZIF-triggered rapid polymerization of dopamine renders Co/N-codoped cage-in-cage porous carbon for highly efficient oxygen reduction and evolution[J]. Nano Energy, 2021, 79: 105487.

[4] Han X, Zheng Z, Chen J, et al. Efficient oxygen reduction on sandwich-like metal@ N–C composites with ultrafine Fe nanoparticles embedded in N-doped carbon nanotubes grafted on graphene sheets[J]. Nanoscale, 2019, 11(26): 12610-12618.

[5] Fan H, Mao K, Liu M, et al. Tailoring the nano heterointerface of hematite/magnetite on hierarchical nitrogen-doped carbon nanocages for superb oxygen reduction[J]. Journal of Materials Chemistry A, 2018, 6(43): 21313-21319.

[6] Wang Z, Xu W, Chen X, et al. Defect-rich nitrogen doped Co_3O_4/C porous nanocubes enable high-efficiency bifunctional oxygen electrocatalysis[J]. Advanced Functional Materials, 2019, 29(33): 1902875.

[7] Cheng Q, Yang L, Zou L, et al. Single cobalt atom and N codoped carbon nanofibers as highly durable electrocatalyst for oxygen reduction reaction[J]. Acs Catalysis, 2017, 7(10): 6864-6871.

[8] Devi B, Koner R R, Halder A. Ni (II)-dimeric complex-derived nitrogen-doped graphitized carbon-encapsulated nickel nanoparticles: efficient trifunctional electrocatalyst for oxygen reduction reaction, oxygen evolution reaction, and hydrogen evolution reaction[J]. ACS Sustainable Chemistry & Engineering, 2018, 7(2): 2187-2199.

[9] Wang B, Ye Y, Xu L, et al. Space-Confined Yolk-Shell Construction of Fe_3O_4 Nanoparticles Inside N-Doped Hollow Mesoporous Carbon Spheres as Bifunctional Electrocatalysts for Long-Term Rechargeable Zinc-Air Batteries[J]. Advanced Functional Materials, 2020, 30(51): 2005834.

[10] Liu X, Li W, Zou S. Cobalt and nitrogen-codoped ordered mesoporous carbon as highly efficient bifunctional catalysts for oxygen reduction and hydrogen evolution reactions[J]. Journal of Materials

Chemistry A, 2018, 6(35): 17067-17074.

[11] Li Y, Huang H, Chen S, et al. 2D nanoplate assembled nitrogen doped hollow carbon sphere decorated with Fe_3O_4 as an efficient electrocatalyst for oxygen reduction reaction and Zn-air batteries[J]. Nano Research, 2019, 12(11): 2774-2780.

[12] Liang Z, Fan X, Lei H, et al. Cobalt-Nitrogen-Doped Helical Carbonaceous Nanotubes as a Class of Efficient Electrocatalysts for the Oxygen Reduction Reaction[J]. Angewandte Chemie, 2018, 130(40): 13371-13375.

[13] Ma L, Wang R, Li Y H, et al. Apically Co-nanoparticles-wrapped nitrogen-doped carbon nanotubes from a single-source MOF for efficient oxygen reduction[J]. Journal of Materials Chemistry A, 2018, 6(47): 24071-24077.

[14] Yang C C, Zai S F, Zhou Y T, et al. Fe_3C-Co nanoparticles encapsulated in a hierarchical structure of N‐doped carbon as a multifunctional electrocatalyst for ORR, OER, and HER[J]. Advanced Functional Materials, 2019, 29(27): 1901949.

[15] Zhang Y, Jiang H, Lin Y, et al. In situ growth of cobalt nanoparticles encapsulated nitrogen‐doped carbon nanotubes among $Ti_3C_2T_x$ (MXene) matrix for oxygen reduction and evolution[J]. Advanced Materials Interfaces, 2018, 5(16): 1800392.

[16] Lemes G, Sebastián D, Pastor E, et al. N-doped graphene catalysts with high nitrogen concentration for the oxygen reduction reaction[J]. Journal of Power Sources, 2019, 438: 227036.

[17] Bian Y, Wang H, Hu J, et al. Nitrogen-rich holey graphene for efficient oxygen reduction reaction[J]. Carbon, 2020, 162: 66-73.

[18] Guo J, Cheng Y, Xiang Z. Confined-space-assisted preparation of Fe_3O_4-nanoparticle-modified Fe-N-C catalysts derived from a covalent organic polymer for oxygen reduction[J]. ACS Sustainable Chemistry & Engineering, 2017, 5(9): 7871-7877.

[19] Wang Z, Xu W, Chen X, et al. Defect-rich nitrogen doped Co_3O_4/C porous nanocubes enable high‐efficiency bifunctional oxygen electrocatalysis[J]. Advanced Functional Materials, 2019, 29(33): 1902875.

[20] Guo H, Feng Q, Zhu J, et al. Cobalt nanoparticle-embedded nitrogen-doped carbon/carbon nanotube frameworks derived from a metal–organic framework for tri-functional ORR, OER and HER electrocatalysis[J]. Journal of Materials Chemistry A, 2019, 7(8): 3664-3672.

[21] Wang R, Yan T, Han L, et al. Tuning the dimensions and structures of nitrogen-doped carbon

nanomaterials derived from sacrificial g-C_3N_4/metal-organic frameworks for enhanced electrocatalytic oxygen reduction[J]. Journal of Materials Chemistry A, 2018, 6(14): 5752-5761.

[22] Mi J L, Liang J H, Yang L P, et al. Effect of Zn on size control and oxygen reduction reaction activity of Co nanoparticles supported on N-doped carbon nanotubes[J]. Chemistry of Materials, 2019, 31(21): 8864-8874.